Original Article

Institution of MECHANICAL ENGINEERS
Journal of MULTI-BODY DYNAMICS

Proc IMechE Part K: J Multi-body Dynamics
2021, Vol. 235(2) 217–234

DOI: 10.1177/1464419320956831
journals.sagepub.com/home/pik
SAGE

Reducing wheel wear from the perspective of rail track layout optimization

Yunguang Ye[1] and Yu Sun[2]

Abstract

Wheel wear (W-wear) is one of the most critical issues affecting vehicle-track performances and operating costs. Currently, the works on W-wear behavior and W-wear reduction are mainly based on four aspects: wheel-rail (WR) tribology, WR profile, vehicle structure design and active control of vehicle suspensions. Little attention has been paid to the effects of track layout parameters, such as superelevation, gauge, and cant. To supplement the existing research, this work aims to investigate the relationship between W-wear and track layout parameters and ultimately reduce W-wear through optimizing track layout parameters. The framework consists of a series of steps. Firstly, a multibody dynamics simulation (MBS) model of an Sgnss wagon with 55 degrees of freedom (DOFs) is built. Then, taking a 375-m-radius curve as a case, the influence of track layout parameter (superelevation, gauge, and cant) on W-wear and vehicle derailment safety is investigated based on Kriging surrogate model (KSM). Finally, based on optimized results obtained by KSM and particle swarm optimization (PSO), two optimal regions and three reasonable suggestions concerning the layout of a 375-m-radius curve are given from the perspective of reducing W-wear. This study is promising for the parameter setting of those dedicated lines, on which the train speed is usually fixed, such as metro, light rail, and tram.

Keywords

Wheel wear, small-radius curve, track layout setting, optimization

Date received: 18 December 2019; accepted: 15 August 2020

Introduction

Existing methods to reduce W-wear

The increase in railway vehicle speed, axle load, and traffic volume exacerbates W-wear, which shortens the wheel re-profiling mileage and deteriorates vehicle-track performances.[1,2] Reducing W-wear, therefore, has been a topic of great interest. At present, the works on W-wear behavior and W-wear reduction are mainly based on four aspects: WR tribology, WR profile, vehicle structure design and active control of vehicle suspensions.

WR tribology. The WR tribology is the most fundamental factor that influences W-wear. An effective way to reduce W-wear is to use materials with excellent wear-resistance properties, such as high hardness materials, or laser surface treatments to steel wheels, including laser dispersion quenching and laser cladding.[3–5] The material with excellent wear-resistance properties, however, is likely to show high sensitivity to rolling contact fatigue (RCF). Also, a relatively small number of standardized steel grades are allowed for wheel manufacturing. The second possibility to reduce W-wear is to change the friction properties of the WR interface. For instance, low friction modifiers or lubricants, such as oils, greases, water, etc., are used to reduce the friction coefficient between wheel flange (WF) and rail gauge corner (GC) (Region B in Figure 1) and keep this value, usually, below 0.2. Then, the wheel flange wear (WF-wear) can be significantly reduced when the vehicle is running on small-radius curves.[6,7]

[1]Institute of Land and Sea Transport Systems, Technical University of Berlin, Berlin, Germany
[2]College of Transportation Science & Engineering, Nanjing Tech University, Nanjing, China

Corresponding authors:
Yunguang Ye, Institute of Land and Sea Transport Systems, Technical University of Berlin, Berlin 10587, Germany.
Email: yunguang.ye@campus.tu-berlin.de
Yu Sun, College of Transportation Science and Engineering, Nanjing Tech University, Nanjing 210009, China.
Email: sunyu.9003@163.com

WR profile. WR contact form is the most critical geometrical factor affecting W-wear. As shown in Figure 1, the WR contact region consists of three sub-regions: (1) *Region A*: wheel tread–rail head (WT-RH). When the wheel rolls on straight tracks or large radius curves, the WR contact usually occurs in this region. This region yields the lowest contact pressures and lateral forces, which results in the most moderate WT-RH wear. (2) *Region B*: wheel flange–gauge corner (WF-GC). The WR contact tends to occur in this region when the wheel rolls on small-radius curves. This region produces severe WF-GC wear because the contact patch is much smaller than that in region A and the sliding velocity is larger. (3) *Region C*: contact between field sides of the wheel and rail. Contact is least likely to appear in this region. The appearance of the contact in this region may cause incorrect steering of the wheelset and severe W-wear. Therefore, letting the WR contact occur primarily in region A is the optimal solution to reduce W-wear, in which, a suitable W-profile plays an important role. The optimization of W-profiles, therefore, is a topic of great concern. Up to now, the methods with different strategies concerning the optimization of W-profiles can be mainly classified into three categories:

Bio-inspired optimization algorithm-based profile designing methods, such as genetic algorithm (GA),[8–11] PSO,[12,13] and Covariance Matrix Adaptation Evolution Strategy (CMA-ES).[14]
Target-based techniques, such as target rolling radius difference (RRD),[15,16] target conicity,[17] target WR normal gap,[18] and target contact angle[19];
Wear model, such as FASTSIM-USFD-based or FaStrip-USFD-based wheel wear calculation method.[20–23]

When designing a profile, several of the listed strategies can be used simultaneously. More information concerning wheel profile optimization-based wheel wear reduction can be found in literature.[20,24]

Vehicle design. Vehicle suspensions and bogie structures can also affect W-wear. In terms of the vehicle suspension, Fergusson et al.[25] studied the longitudinal and lateral primary suspension stiffness and the centre plate friction of a self-steering three-piece bogie. The results showed that a reasonable combination of these three parameters could reduce the wear number by up to 50%. Mazzola et al.[26] investigated the influence of suspension system parameters on the W-wear of a non-powered high-speed car. In their work, the longitudinal and lateral stiffnesses of the primary suspension and the yaw damper coefficient of the secondary system were investigated. The results showed that different combinations of these three parameters had a different influence on the wear index. In terms of the bogie structure, Mazzola et al.[26] studied the influence of the wheelbase on the W-wear, the simulation results showed that a shorter wheelbase yielded a lower wear index. Bideleh et al.[27] explored the influence of the arrangement of suspension systems on the wear number, where an asymmetric suspension system presented remarkable benefits in wear reduction when the vehicle operated on small-radius curves. The Lewis[2] concluded that the articulated bogie, the bogie with a shorter wheelbase and the radial bogie could reduce W-wear. The root cause was that these three structural forms could reduce the attacking angles of wheelsets as well as the guiding forces.

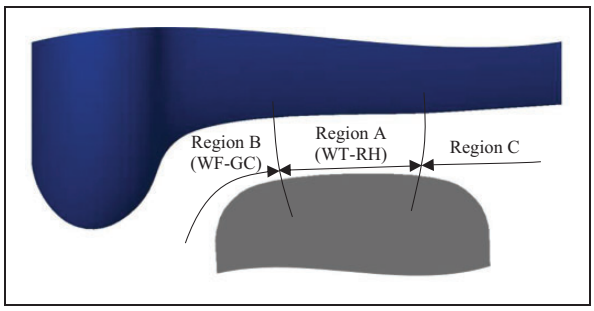

Figure 1. WR contact regions.

Active control of vehicle suspension. Up to now, most of the studies concerning W-wear reduction are based on passive vehicles. The active suspension system is more effective in reducing W-wear since it controls the attacking angles of wheelsets and the guiding forces. This technology can greatly reduce the wheel flange wear (WF-wear) when the vehicle is running on small-radius curves. For active primary suspensions, Pérez et al.[28] showed that a vehicle with active primary suspensions could reduce the wear index on a curve by a factor of 5 relative to a vehicle with passive primary suspensions. For active secondary suspensions, full-scale tests performed on a bogie using the NTSEL roller rig test stand in Japan[29] showed that the use of active secondary suspensions could reduce guiding forces on small-radius curves.

Motivation

In addition to the aforementioned studies, many other studies have contributed to W-wear reduction.[30–32] The vehicle-track system, however, is huge and complex; it is difficult to study W-wear systematically. Most of these studies have aimed at reducing W-wear on curves with an ideal radius,[33] with little attention to the track layout parameters, such as superelevation, gauge, and cant.

Concerning the influence of track layout parameters on W-wear, Gao et al.[34] studied the superelevation setting for a curve with a 400-m-radius curve of the China Shen-Shuo railway line based on Hertzian theory and FASTSIM algorithm. The simulation

results showed that reducing the superelevation appropriately could reduce wear power. Based on the simulation result and taking into account the actual operating condition, they proposed to decrease the superelevation of the curve by 10 mm. Furthermore, field experiments proved the correctness of this modification. Pombo et al.[35] investigated the influence of rail cant on W-wear growth, in which the W-profile S1002 and the rail profile UIC60 were used. The results revealed that the reprofiling intervals obtained when running on the track with a rail cant of 1:40 were larger than when traveling on a track with a rail cant of 1:20. It indicated that the use of a rail cant of 1:40 is advantageous in terms of W-wear progression compared with a rail cant of 1:20. Based on the FASTSIM-Archard model, Li et al.[36] analyzed the influence of track layout on W-wear by taking a high-speed train with the S1002CN-RF wheel profile as an example. The results showed that different cant deficiencies would cause different wear distribution forms and different wear rates of the wheel.

Besides, as far as the authors know, there are few other studies on the relationship between track layout parameters and W-wear, and further research is needed. More importantly, in practice, to allow the train to pass through a small-radius curve smoothly, both the superelevation and gauge of the curve need to be properly adjusted, such as setting the superelevation close to the equilibrium superelevation, or widening the gauge. Investigating the influence of simultaneous changes in superelevation and gauge on the wheel and/or rail wear and ultimately optimizing these parameters to reduce wear, therefore, is also a topic of big interest in terms of extending wheel and/or rail life and reducing operating costs, especially for the small-radius curved tracks.

Proposed method

For discrete datasets, parameter optimization often needs to be built on a large amount of sampled data. Specifically, for multi-body dynamics simulation, a lot of repetitive modeling is required. For instance, in Firlik et al.,[14] to find a wheel profile that takes into account the wear index, the derailment coefficient, and the wheel-rail contact patch area, over 50 000 wheel profiles were evaluated. The railway industry is reluctant to do many deterministic analyses. Besides, the test process involves steps such as numerical calculation, analysis, etc., involving a large number of uncertainties. It not only consumes much human labor but also may increase errors.[37–39]

Alternatively, the surrogate model (SM) technique can overcome the above two shortages. It is an approximate mathematical model with low computational complexity and high computational accuracy. It uses a small number of sample points that meet specific sampling strategies to construct a simplified mathematical model that approximates the original complex model. The SM technique, therefore, can replace the original analytical model and simplify the calculation process while maintaining high calculation accuracy. In our work, the KSM technique,[40] which is an unbiased estimation model that fully considers the spatial correlation of variables, is used to model the relationship between track layout parameters and W-wear. After obtaining the response relationship between track layout parameters and W-wear, the track layout optimization issue is finally transformed into an inverse problem of solving the established KSM, this means that the optimal track layout parameters can be found by the information of the lowest W-wear value. To achieve automatic optimization, the PSO[41] algorithm is applied.

Contribution and structure of this paper

The main work of this paper is summarized as follows:

1. A vehicle/track coupled dynamics model is established, in which the wheelset and track flexibilities are considered.
2. Taking a 375-m-radius curve as a case, the influence of track layout parameters (superelevation, gauge, and cant) on W-wear and vehicle derailment safety is investigated based on the KSM technique.
3. A KSM-PSO based track layout parameter optimization method is proposed, and two optimal regions for track layout parameter setting for reducing W-wear are presented.
4. Three suggestions concerning track layout are given from the perspective of reducing W-wear.

The rest of this paper is structured as follows. In the next section, a vehicle/track coupled dynamics model is established. Then, the theory of KSM and the optimization problem is described. In the 'Experimental result' section, firstly, taking a 375-m-radius curve as an example, the influence of track layout parameters (superelevation, gauge, and cant) on W-wear and derailment safety is studied based on KSM. Then, the optimal track layout for reducing W-wear is found based on PSO. Finally, an optimal region and three suggestions for the track layout setting are given. In the penultimate section, based on the Hertzian-FaStrip-USFD wear calculation method, an optimized track layout is introduced as a case to compare with a normal track layout. The wear distribution shows that the optimized track layout can greatly reduce the WF-wear and make the wheel tread wear (WT-wear) more uniform. Conclusions and discussion are drawn in the final section.

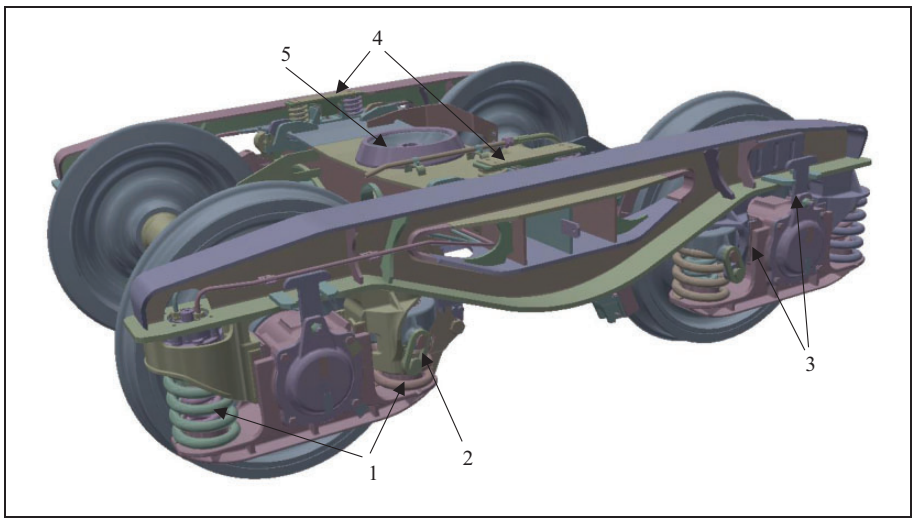

Figure 2. 3 D view of the Y25 bogie.

Vehicle/track coupled dynamics model

Vehicle model

The vehicle used in our work is an Sgnss wagon with two Y25 bogies. The model consists of three substructures, one for the carbody and two for the bogies. Since the bogie is the most important part of a railway vehicle from the perspective of dynamics, it is detailedly described here. As shown in Figure 2, the bogie has two stages of suspensions, i.e., the primary suspension and the fake secondary suspension.

The primary suspension, which links the axlebox with the bogie frame, is made up of:

- Two flexi-coil spring sets (per axlebox), where each spring set has two nested coil springs, i.e., an inner coil spring and an outer coil spring;
- An inclined Lenoir link (per axlebox), to connect the bogie frame and the spring holder;
- A nonlinear longitudinal bump stop (per axlebox), to limit the longitudinal displacement of the axlebox;
- A nonlinear lateral bump stop (per axlebox), to limit the lateral displacement of the axlebox;
- A nonlinear vertical bump stop (per axlebox), to limit the vertical displacement of the axlebox.

There is no real secondary suspension on the Y25 bogie. The fake secondary suspension, which connects the bogie frame and carbody, is made up of:

- Two sprung side bearers, to provide friction damping in yaw and restraint in roll;
- A spherical central pivot, only allowing three rotational DOFs;
- A nonlinear longitudinal bump stop (per side bearer), to limit the longitudinal displacement of the bogie frame;
- A nonlinear vertical bump stop (per side bearer), to limit the vertical displacement of the bogie frame.

The WR impact forces may contribute to the elastic deformation of the wheelset, which could subsequently alter the characteristics of the WR contact force.[42,43] Therefore flexible wheelset is considered in this work. The wheelset is firstly modeled as a rigid body in INVENTOR and then imported into ANSYS to calculate its flexible modes. Finally, the first 30 eigenmodes belonging to eigenfrequencies up to 1006.3 Hz are imported into SIMPACK via the finite element multibody systems (FEMBS) interface. Figure 3 presents some of the flexible mode shapes of the wheelset together with the corresponding frequencies.

Finally, the whole vehicle model is made up of 15 bodies (one rigid carbody, two rigid bogie frames, eight rigid axleboxes, and four flexible wheelsets) and 90 force elements, with 55 DOFs in total. In our work, the bogie-related parameters were obtained from the laboratory tests. All the springs, dampers and friction elements are modeled using non-linear characteristics as well as algebraic and logical equations. Moreover, the accuracy of these parameters was verified by using the actual test data.[44] The MBS model of the whole vehicle and the bogie, and the data of interest are shown in Figure 4 and Table 1, respectively. More information concerning the MBS model, including the detailed modeling steps and force elements, can be found in the authors' previous work.[45–47]

Wheelset-track model

The wheelset is supported by two rails, where the Hertzian contact and FASTSIM algorithms are used. The track flexibility is also considered in the model, and the topology diagram of the wheelset-track model is shown in Figure 5, where the track model is made up of two rails, discrete sleepers, and a ground. The stiffness and damping of the fastener

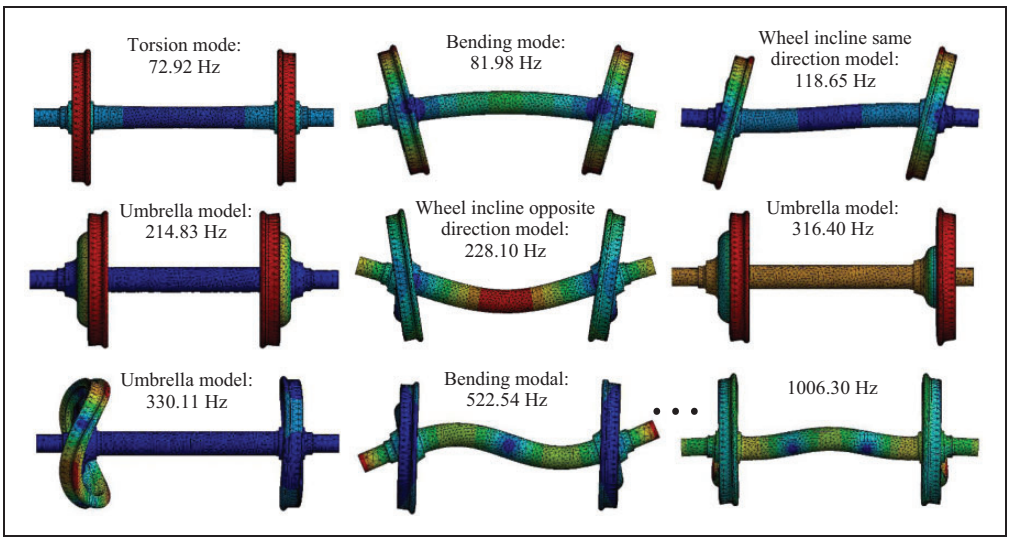

Figure 3. Selected vibration modes of the flexible wheelset together with the corresponding frequencies.[38]

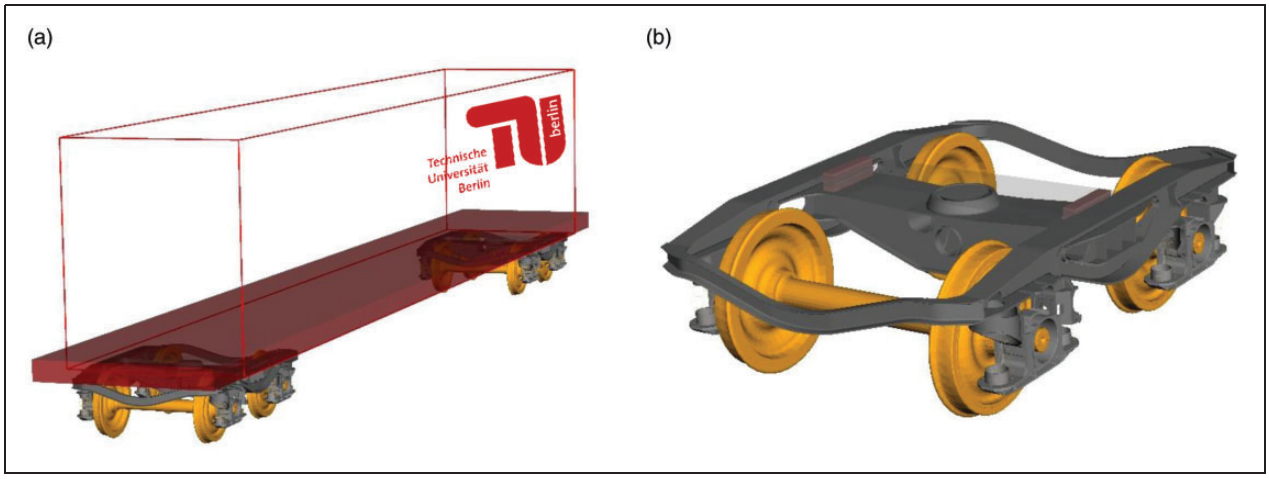

Figure 4. The vehicle model (a); and the Y25 bogie (b).

are considered between rails and sleepers, and the stiffness and damping of the ballast are considered between sleepers and ground. The parameters are listed in Table 1.

KSM-PSO-based track layout optimization method for reducing W-wear

KSM

The basic idea of KSM is to use a small number of sample points that meet specific sampling strategies to construct a simplified mathematical model that approximates the original complex model. This technique has two main functions:

- The solution of the unknown region is predicted due to its nonlinear regression ability. Therefore, it can be used to simplify engineering calculations.[37] This is a forward solution strategy.
- Optimization tool. The optimization target is considered as the model response, and the optimization algorithm is used to perform the optimization calculation. This is a reverse solution strategy.

In our work, KSM[40] is applied as the optimization tool to model the relationship between track layout parameters and W-wear, in which, the track layout parameters and W-wear are considered as input variables and model response, respectively.

Assuming that the response value corresponding to the sample point group $\mathbf{X} = \{x_1, x_2, \ldots, x_n\}$ is $\mathbf{Y} = \{y(x_1), y(x_2), \ldots, y(x_n)\}$, the relationship between the input variables and their response can be expressed[37]

$$y(\mathrm{x}) = f^{\mathrm{T}}(\mathrm{x})\boldsymbol{\beta} + Z(\mathrm{x}) \tag{1}$$

Table 1. Primary parameters of the vehicle-track model.

Parameter	Value	Unit
Vehicle frame mass (m_v)	70 000	[kg]
Bogie frame mass (m_b)	1887	[kg]
Axlebox mass (m_a)	152	[kg]
Wheelset mass (m_w)	1121	[kg]
Sleeper mass (m_s)	330	[kg]
Carbody roll moment of inertia (I_{cxx})	7399	[kg m^2]
Carbody pitch moment of inertia (I_{cyy})	1 998 266	[kg m^2]
Carbody yaw moment of inertia (I_{czz})	2 418 154	[kg m^2]
Bogie frame roll moment of inertia (I_{bxx})	1188	[kg m^2]
Bogie frame pitch moment of inertia (I_{byy})	1484	[kg m^2]
Bogie frame yaw moment of inertia (I_{bzz})	2582	[kg m^2]
Axlebox roll moment of inertia (I_{axx})	2.18	[kg m^2]
Axlebox pitch moment of inertia (I_{ayy})	7.57	[kg m^2]
Axlebox yaw moment of inertia (I_{azz})	6.71	[kg m^2]
Wheelset roll moment of inertia (I_{wxx})	592.9	[kg m^2]
Wheelset pitch moment of inertia (I_{wyy})	96.34	[kg m^2]
Wheelset yaw moment of inertia (I_{wzz})	592.9	[kg m^2]
Pivot distance ($2a^*$)	14.2	[m]
Wheelset base ($2a^+$)	1.8	[m]
Wheel rolling circle diameter (D)	920	[mm]
Secondary suspension damping (c_{sx}, c_{sy} and c_{sz})	10	[kNs/m]
Fastener damping (c_{fy} and c_{fz})	5.5 and 63	[kNs/m]
Ballast damping (c_{by} and c_{bz})	49 and 94	[kNs/m]
WR contact damping (c_c)	10	[kNs/m]
Fastener stiffness (k_{fy} and k_{fz})	1700 and 280 000	[kN/m]
Ballast stiffness (k_{by} and k_{bz})	20,000 and 75 000	[kN/m]
Contact stiffness (k_c)	According to the non-linear wheel/rail contact model (Hertzian contact)	—
The friction coefficient between wheels and rails (μ)	0.35	—
Poisson ratio (υ)	0.28	—
Wheel profile	S1002	—
Rail profile	UIC60e1	—
Track irregularities.	ERRI B176	

where $y(\mathrm{x})$ is the predicted response, $f^{\mathrm{T}}(\mathbf{x})$ is the regression model founded by the known function that depends on $\mathbf{x}$, $\boldsymbol{\beta}$ is an undetermined coefficient, $Z(\mathbf{x})$ is a random Gaussian distribution with a mean of zero and variance of σ^2. The covariance matrix of $Z(\mathbf{x})$ for a m-variable design space can be expressed as equation (2):

$$\begin{aligned} &\mathrm{Cov}\left[Z(\mathrm{x}^{(i)}), Z(\mathrm{x}^{(j)})\right] = \sigma^2 R\left(\theta, \mathrm{x}^{(i)}, \mathrm{x}^{(j)}\right), \text{ and} \\ &R\left(\theta, \mathrm{x}^{(i)}, \mathrm{x}^{(j)}\right) = \exp\left[-\sum_{l=1}^{m} \theta_l \left| x_l^{(i)} - x_l^{(i)} \right|^2\right] \end{aligned} \tag{2}$$

where $\mathrm{x}^{(i)}$ and $\mathrm{x}^{(\mathrm{j})}$ are two sample points in the sample space, and $1 \le i,j \le n$; $R\left(\theta, \mathrm{x}^{(\mathrm{i})}, \mathrm{x}^{(\mathrm{j})}\right)$ represents the spatial correlation between the sample points $\mathrm{x}^{(\mathrm{i})}$ and $\mathrm{x}^{(\mathrm{j})}$; $x_l^{(i)} - x_l^{(i)}$ represents the absolute distance between $x_l^{(i)}$ and $x_l^{(i)}$; θ_l is the lth component of θ, which indicates how active a variable is in the surrogate model. Larger values of θ_{l} can be interpreted as high-level of activity while small values of θ_{l} indicate that the variable can be ignored in the surrogate model, $1 \le l \le 2$ in this paper. Therefore, a correlation matrix between the sample points and their response values can be obtained, as

$$R = \begin{bmatrix} R\left(\theta, \mathrm{x}^{(1)}, \mathrm{x}^{(1)}\right) & \cdots & R\left(\theta, \mathrm{x}^{(1)}, \mathrm{x}^{(n)}\right) \\ \vdots & \ddots & \vdots \\ R\left(\theta, \mathrm{x}^{(n)}, \mathrm{x}^{(1)}\right) & \cdots & R\left(\theta, \mathrm{x}^{(n)}, \mathrm{x}^{(n)}\right) \end{bmatrix} \tag{3}$$

Therefore, the value of θ needs to be determined firstly, it can be calculated by maximizing the likelihood estimate of the response value, as

$$ln(\theta) = -\frac{1}{2}\left[n\ln\hat{\sigma}^2 + \ln\mathrm{R} + \frac{1}{\hat{\sigma}^2}\left(\mathrm{Y} - \mathrm{f}^{\mathrm{T}}\hat{\beta}\right)^{\mathrm{T}}\mathrm{R}^{-1}\left(\mathrm{Y} - \mathrm{f}^{\mathrm{T}}\hat{\beta}\right)\right] \tag{4}$$

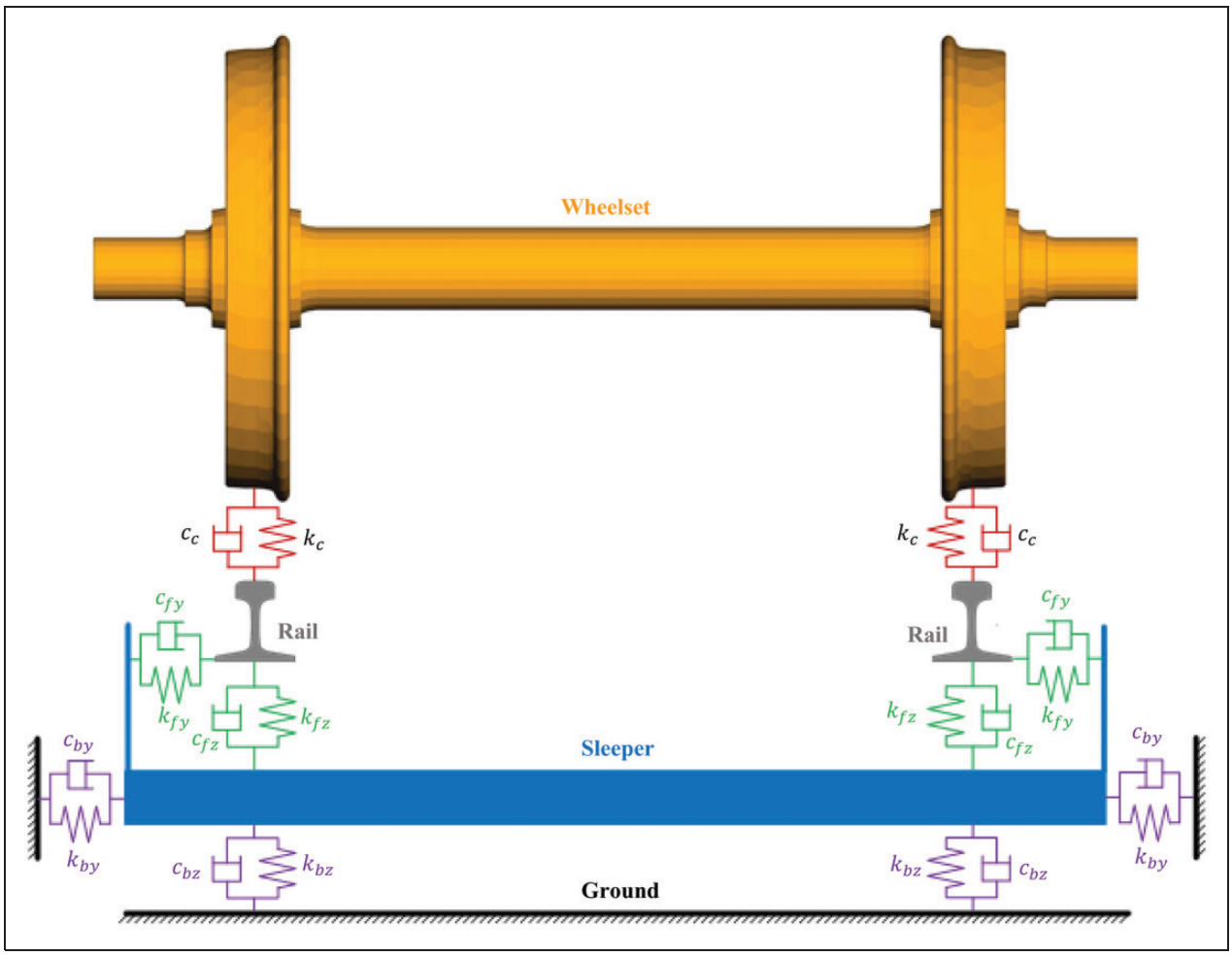

Figure 5. The topology of the wheelset-track model.

The estimation of θ depends on $\hat{\beta}$ and $\hat{\sigma}^2$. $\hat{\beta}$ and $\hat{\sigma}^2$ can be calculated using the generalized least square method, and given as

$$\hat{\beta} = (\mathrm{F}^{\mathrm{T}}\mathrm{R}^{-1}\mathrm{F})^{-1}(\mathrm{F}^{\mathrm{T}}\mathrm{R}^{-1}\mathrm{Y}) \tag{5}$$

$$\hat{\sigma}^2 = \frac{1}{n}\left(\mathrm{Y} - \mathrm{F}^{\mathrm{T}}\hat{\beta}\right)^{\mathrm{T}}\mathrm{R}^{-1}\left(\mathrm{Y} - \mathrm{F}^{\mathrm{T}}\hat{\beta}\right) \tag{6}$$

where $\mathbf{F} = [f(\mathrm{x}^{(1)}), f(\mathrm{x}^{(2)}), \ldots, f(\mathrm{x}^{(n)})]^{\mathrm{T}}$.

Finally, after determining the input information of the unknown point $\mathbf{x}$, the corresponding response value of the point $\mathbf{x}$ can be predicted by the KSM using equation (7):

$$\hat{y}(\mathrm{x}) = F^{\mathrm{T}}(\mathrm{x})\hat{\beta} + r(\mathrm{x})^{\mathrm{T}}\mathrm{R}^{-1}\left(\mathrm{Y} - \mathrm{F}\hat{\beta}\right) \tag{7}$$

where $r(\mathrm{x}) = [R(\theta, \mathrm{x}, \mathrm{x}^{(1)}), R(\theta, \mathrm{x}, \mathrm{x}^{(2)}), \ldots, R(\theta, \mathrm{x}, \mathrm{x}^{(n)})]$ represents the correlation function vector of the sample point to be tested and each known sample point. This term relates $\hat{y}$ to the absolute distance between the new point and the sampled data, so the uncertainty of the predicted value must be minor if the new point is sufficiently close to one of the sampled points. On the other hand, the uncertainty of the predicted value for a far-located point is significant. Here, the Mean Squared Error (MSE), which is again dependent on r, is used to measure the uncertainty of the predicted value, see equation (8):

$$\hat{s}^2(\mathrm{x}) = \hat{\sigma}^2\left[1 - \mathrm{r}^{\mathrm{T}}\mathrm{R}^{-1}\mathrm{r} + \frac{(1 - 1^{\mathrm{T}}\mathrm{R}^{-1}\mathrm{r})^2}{1^{\mathrm{T}}\mathrm{R}^{-1}\mathrm{r}}\right] \tag{8}$$

where the term $(1 - 1^{\mathrm{T}}\mathrm{R}^{-1}\mathrm{r})^2/(1^{\mathrm{T}}\mathrm{R}^{-1}\mathrm{r})$ is often ignored since it is a higher-order small-term.[37] The square root of equation (8) (RMSE) is usually used as an index for measuring the accuracy of a surrogate model over the design space. To achieve the aim of unbiased estimation, the RMSE value should be kept to a minimum. If this value is large, it means that the accuracy of the KSM is low. Therefore, more samples are required to construct a new KSM model.

Because the KSM has local and global statistical properties, high-precision fitting effects can be achieved when solving nonlinear problems.

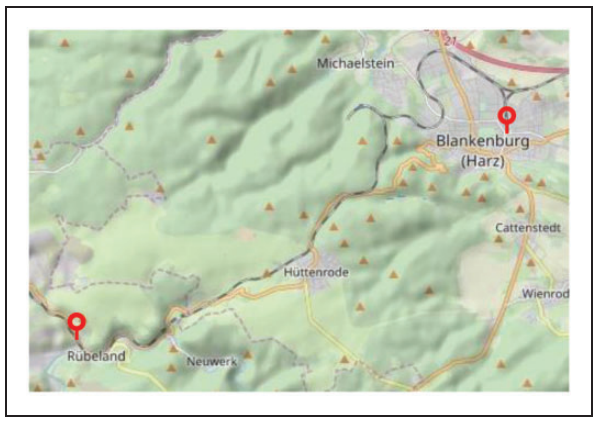

Figure 6. Rübeland-Blänkenburg railway line.

Optimization problem statement

The Blankenburg-Rübeland line (Figure 6) is located in the Harz Mountains in Germany, connecting the companies located there to the railway network, such as Hüttenwerke and Kalkbranntwerke.[48] The line currently mainly undertakes the lime transportation task of the Fels-Werke GmbH in Harz. As shown in Figure 4, this line contains many tight curves which result in severe W-wear, increasing the maintenance costs and threatening the running safety.

We found that the wear of train wheels running on this line was extremely serious. Our work, therefore, takes a 375-m-radius curve of this line as an example to study the effects of track layout parameters on W-wear. The vehicle speed was about 51 km/h. The data concerning the track and the Sgnss wagon, as well as the vehicle speed, were supported by the DynoTRAIN project, which was funded by the European Commission.

Design variables. When a train is running on a curve, due to the centrifugal force, the wear between the wheel and rail is much more serious than when running on a straight line. To balance the centrifugal force of the train on a curve, the outer rail of the curved section needs to be set higher than the inner rail, i.e. superelevation (Figure 7). The superelevation S (mm) is determined according to the curve radius r (m) and the train speed v (km/h). When the value meets equation (9), the centripetal force provided by the superelevation can balance the entire centrifugal force, and the superelevation at this time is called the equilibrium superelevation. Setting the superelevation reasonably can reduce WR wear and prolong the service life of the wheel and rail. Conversely, too high or too low will affect operational safety.

$$S_e = 11.8\frac{v^2}{r} \tag{9}$$

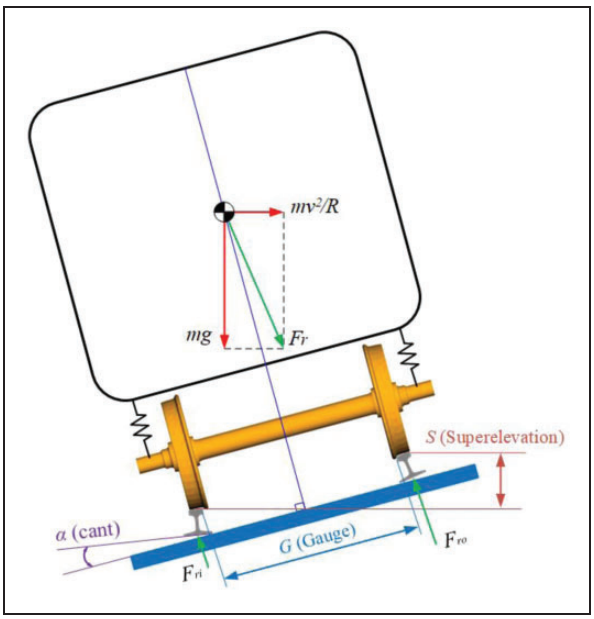

Figure 7. Sketch of the superelevation, gauge, and cant of a curved track.

The tack gauge is defined as the distance between the inner sides of the rails measured 14 mm below the rolling surface (Figure 7). Currently, there are some different used gauges worldwide, such as standard gauge ($G = 1.435$ m), metric gauge ($G = 1.000$ m or $G = 1.067$ m) and broad gauge ($G = 1.524$ m in Russia, $G = 1.672$ m in Spain). Among them, the standard gauge is the most widely used. On curves below 400 m radius, it may be necessary to widen the gauge to ease the movement of vehicles and reduce WR wear. For instance, when the radius is between 350 m ~ 400 m, it is recommended to set the track gauge to 1.440 m for the standard gauge. More information concerning this part can be found in Profillidis.[49]

In most cases, rails are mounted with an inclination inwards to fit together with coned W-profiles. Usually, the rail cant α (Figure 7) varies between 1:40 and 1:20, but in some turnouts, rails may be mounted with different inclination.[35] In the German railway network, a 1:40 rail cant is usually used.

In our work, the superelevation and gauge are defined as the design variables of the KSM-based W-wear model; they range from $S_e - 0.4\text{m} \le S_e \le S_e + 0.4\text{m}$ and $1.440\,\text{m} \le G \le 1.460\,\text{m}$, respectively. Besides, the influence of two rail cants ($\alpha = 1:40$, and $\alpha = 1:20$) on W-wear is also investigated.

Optimization objective. Wear of the wheel is a natural process in which the material is removed from the surface of the wheel when the vehicle is running. Currently, there are some $T\gamma$-based models that have been used to predict the wear amount of railway wheels,[50–55] such as BRR model,[50] Zobory model,[51] USFD model,[52] in which, the first step is to calculate the dissipated energy in the WR contact patch. This is

based on the assumption that there is a direct relationship between material loss and energy dissipation. Energy dissipation is expressed as the product of the tangential force (T) and the creepage (γ) in the WR contact patch, i.e., $T\gamma$

$$T\gamma = F_x v_x + F_y v_y \tag{10}$$

where F_x and F_y are the longitudinal and lateral creep forces, respectively; v_x and v_y are the longitudinal and lateral creepages, respectively.

Since the 1st wheelset is a guiding wheelset, and whose WR interaction forces, usually, are greater than the other wheelsets, the average $T\gamma$ value of the first wheelset of the Sgnss wagon after driving 1 km is considered as the optimization target. Finally, the objective function to reduce W-wear can be expressed as

$$f_{\text{wear}}|\min(T\gamma) = \frac{1}{s_t}\int_{t_s}^{t_e}\left(T\gamma_l(t) + T\gamma_r(t)\right)\mathrm{d}t \tag{11}$$

where $T\gamma$ denotes the wear number calculated by KSM; s_t represents the full length of the simulated track, in our work, it is set as 1 km; t_s and t_e represent the start and end simulation time, respectively; $T\gamma_l(t)$ and $T\gamma_r(t)$ are the $T\gamma$ value of the left and right wheel of the first wheelset, respectively.

Constraint function. For small-radius curves, derailment safety is extremely important. The constraint functions introduced in our work refer to the standard,[56] where the derailment coefficient Y/Q and maximal lateral force Y are introduced as constraints to accommodate the dynamic performance of railway vehicles.

Nadal's coefficient is used for estimating the vehicle's running safety and is expressed as

$$\frac{Y}{Q} = \frac{\tan\alpha - \mu}{1 + \mu\tan\alpha} \tag{12}$$

where Y is the vertical force on the wheel; Q is the lateral force on the wheel; α is the wheel flange angle, and μ is the friction coefficient between the wheel and the rail.

The railway must be designed to avoid or minimize the occurrence of any lateral force that is detrimental to the structural safety of the wheel and rail under standard track conditions. The limit of the lateral force is defined as

$$(Y_{2m})|\min = \frac{P_0}{3} + 10\ (\text{kN}) \tag{13}$$

where $Y_{2\,m}$ is the lateral force-sliding mean over 2 m of the track, and P_0 is a static axle load.

After KSM is established, the optimal track layout combination for reducing W-wear can be sought by an automatic optimization method. In this step, PSO[41] is introduced. Finally, the optimization problem is transformed into

$$\begin{cases} \text{Minimize}: & f_{\text{wear}} \\ \text{Subject to}: & \dfrac{Y}{Q} \le 0.8 \\ \text{Subject to}: & Y \le 74.9\ \text{kN} \\ & 0.040\ \text{m} \le S \le 0.120\ \text{m} \\ & 1.440\ \text{m} \le G \le 1.460\ \text{m} \end{cases} \tag{14}$$

Experimental result

Study on the influence of track layout parameters on W-wear and derailment safety base on KSM

When the vehicle is running on a small-radius curve, a two-point contact tends to occur on the outer wheel, which makes the WR interaction extremely complicated and difficult to be analyzed by analytical methods. Therefore, this paper studies the track layout parameters based on the MBS technique. Figure 8 shows the WR contacts of the 1st wheelset when the Sgnss wagon negotiates a 375-m-radius curve with a speed of 51 km/h; it clearly shows that a WF-TH contact occurs on the inner wheel (inner WT-RH contact), while two contacts occur on the outer wheel, i.e., outer WT-RH contact and outer WF-GC contact. In this section, the wear number of these three contacts, as well as the total wear number, are analyzed. Besides, the safety-related indexes, including the derailment coefficient and maximal WR lateral force, are also discussed.

Making a sampling plan. The first step in KSM modeling is to select samples. The sampling plan should consider the following two aspects:

- On one hand, as many samples as possible need to be selected to ensure the accuracy of the KSM. However, when the number of samples reaches a certain level, increasing the sample points will increase the calculation amount instead of improving the accuracy of the model.
- If a desirable point is located far from the sampled points, the accuracy of the approximation may decrease. Therefore, it is necessary to ensure that the sample points can uniformly fill the entire design space, thereby reducing the phenomenon that the local cannot be fitted.

Classical sampling strategies include orthogonal experimental design,[57] Latin hypercube sampling (LHS),[58] uniform experimental design,[59] etc. In this

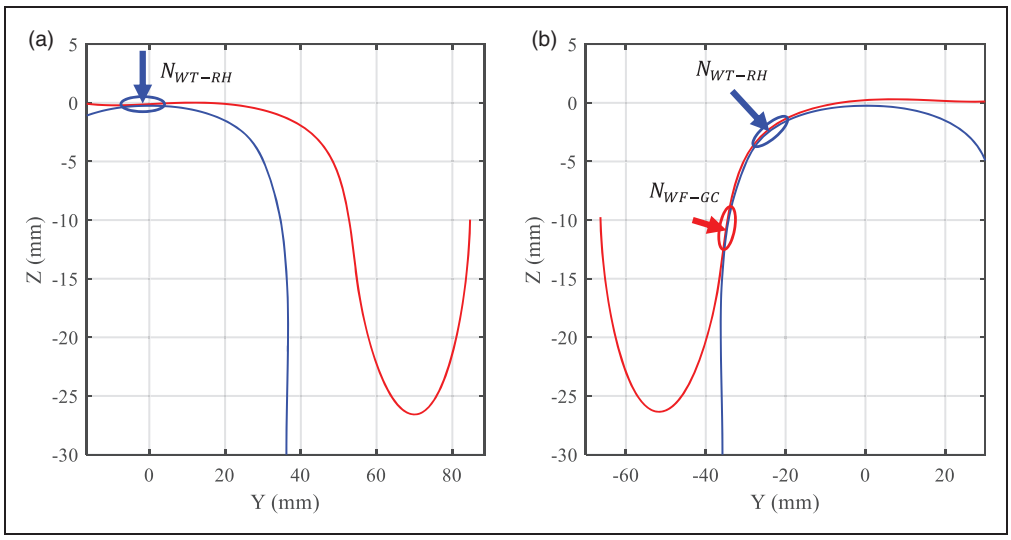

Figure 8. The WR contacts of the 1st wheelset when an Sgnss wagon negotiates a 375-meter-radius curve ($v = 51$ km/h, $S = 0.080$ m, $G = 1.440$ m and $\alpha = 1:40$): (a) inner WT-RH contact and (b) outer WT-RH contact and outer WF-GC contact.

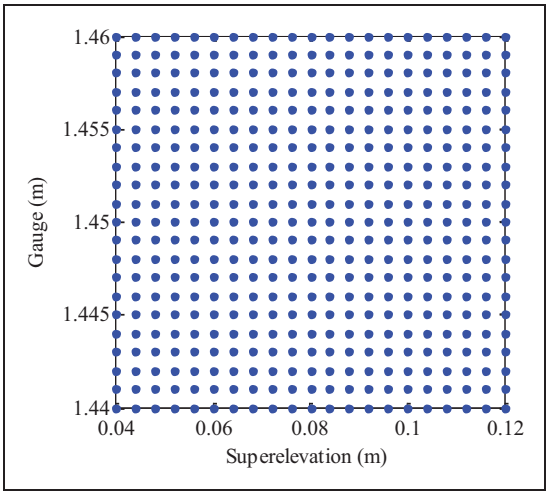

Figure 9. The sampling plan for the KSM.

research, the uniform experimental design sampling strategy with a 21 × 21 matrix is used, with a total of 441 sample points, as shown in Figure 9.

Result analysis. Finally, the KSM-based results, when the rail cant is $\alpha = 1:40$, are shown in Figure 10. It can be seen that there is a nonlinear and non-monotonic relationship between W-wear, derailment safety indicators, and track layout parameters,

Figure 10(a) to (d) shows the result of W-wear when the rail cant is $\alpha = 1:40$, and the following phenomena can be obtained:

- In terms of the inner wheel tread wear (inner WT-wear) (Figure 10(a)), when the gauge is between 1.440~1.450 m, it increases gradually with an increase in superelevation and then begins to increase rapidly at a position near the equilibrium superelevation ($S = 0.080$ m). However, when the gauge is between 1.450~1.460 m, it decreases firstly and then increases.
- In terms of the outer WT wear (outer WT-wear) (Figure 10(b)), no matter which range the gauge is in, overall, it increases as the superelevation increases. Besides, as the gauge widens, it also increases.
- In terms of the outer wheel flange wear (outer WF-wear) (Figure 10(c)), when the gauge is between 1.440~1.450 m, it gradually decreases first and then rapidly increases, reaching a minimum when the superelevation is around 0.068 m. When the gauge is between 1.440~1.450 m, the wear number exhibits a phenomenon of consistently increasing. Also, widening the gauge can significantly decrease the outer WF-wear, and when the gauge is widened to 1.460 m, the outer WF-wear is decreased to about 0.
- In terms of the total wear of the 1st wheelset (Figure 10(d)), its changing tendency is almost the same as that of the outer WF-wear.

Figure 10(e) and (f) shows the safety-related indicators when the rail cant is $\alpha = 1:40$, and the following phenomena can be obtained:

- In terms of the maximal derailment coefficient (Figure 10(e)), both the gauge and the superelevation affect the derailment. Among them, regardless of the range of the gauge, the derailment coefficient decreases first and then increases with the increase of the superelevation. The outer WT number gradually increases with the increase of the superelevation, reaching a minimum when the superelevation increases to near the equilibrium value. However, there is a monotonic relationship between the derailment coefficient and gauge: it decreases as the gauge widens.

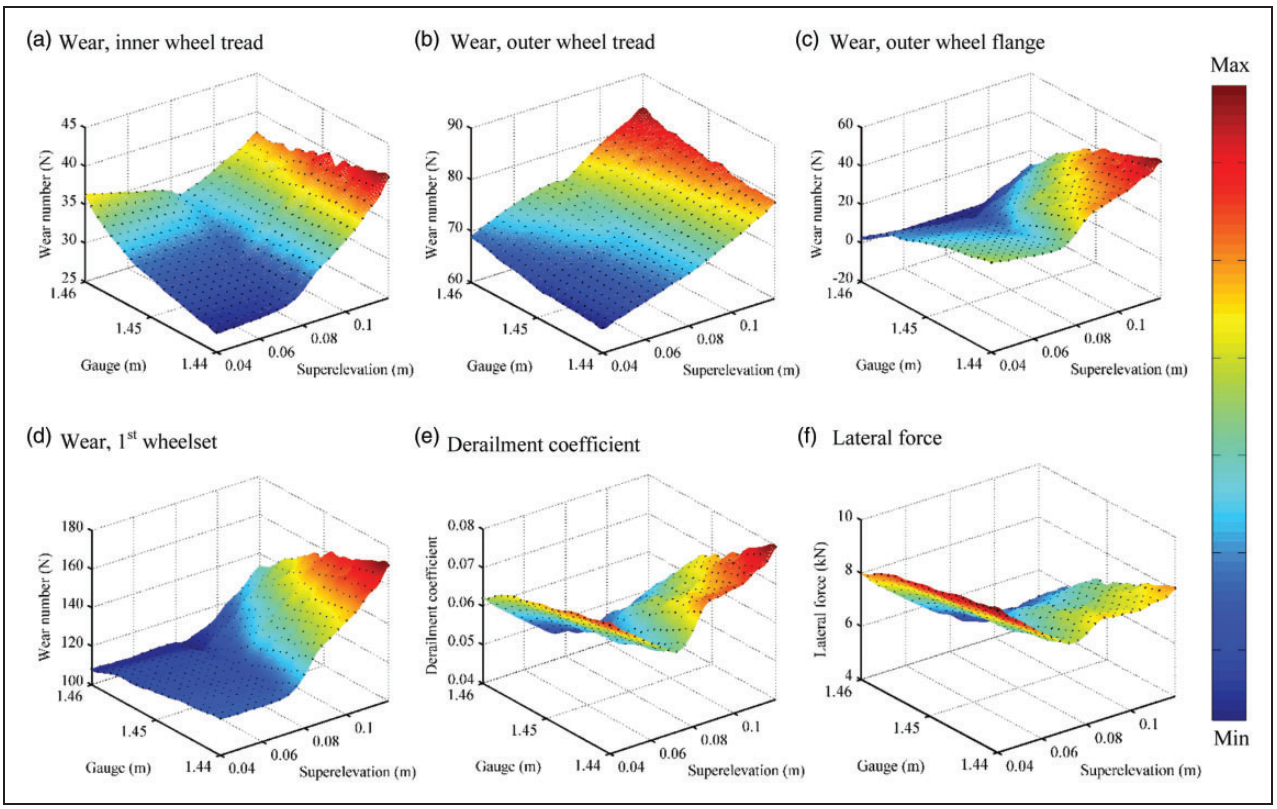

Figure 10. Calculation results when the vehicle negotiates a 375-m-radius curve with a cant of $\alpha = 1 : 40$.

- In terms of the maximal WR lateral force (Figure 10(f)), its changing tendency is almost the same as that of the derailment coefficient.
- These two derailment safety indicators meet the standard[56] since the track layout parameters are only fine-tuned within the scope of safety.

The value of rail cant may be different under different working conditions. The most commonly used value in Germany is $\alpha = 1 : 40$, but $\alpha = 1 : 20$, sometimes, is also used. Therefore, a case with a rail cant of $\alpha = 1 : 20$ is also introduced, and the KSM-based results are shown in Figure 11. It clearly shows that the results under these two cant values are completely different, and the use of a rail cant of $\alpha = 1 : 20$ is worse in terms of W-wear progression compared with a rail cant of $\alpha = 1 : 40$.

Figure 11(a) to (d) shows the result of W-wear when the rail cant is $\alpha = 1 : 20$, and the following phenomena can be obtained:

- In terms of the inner WT-wear (Figure 11(a)), as the superelevation increases, it increases first. When the superelevation increases to about the equilibrium value, it begins to show a slight decrease, and then continues to increase slowly. However, as the gauge is widened, it exhibits a continuous decreasing trend.
- In terms of the outer WT-wear (Figure 11(b)), the outer WF-wear (Figure 11(c)) and the total wear of the 1st wheelset (Figure 11(d)), as the superelevation increases, it first decreases slowly, then sharply decreases in the vicinity of the equilibrium value, and then continues to decrease gradually. However, there is a nearly monotonic relationship between their values and the gauge; they all decrease as the gauge widens.

Figure 11(e) and (f) shows the safety-related indicators when the rail cant is $\alpha = 1 : 20$, and the following phenomenon can be obtained:

- In terms of the maximal derailment coefficient Figure 11(e), as the superelevation increases, it first increases slowly, then sharply increases in the vicinity of the equilibrium value, and then continues to increase gradually. However, there is a monotonic relationship between the derailment coefficient and gauge: it decreases as the gauge widens.
- In terms of the maximal WR lateral force Figure 11(f), as the superelevation increases, it first decreases, then increases in the vicinity of the equilibrium value, and then decreases again. However, there is a nonlinear and non-monotonic relationship between the derailment coefficient and gauge.

KSM-PSO based track layout optimization

KSM verification. To ensure the correctness of the calculation result, the accuracy of the KSM should be

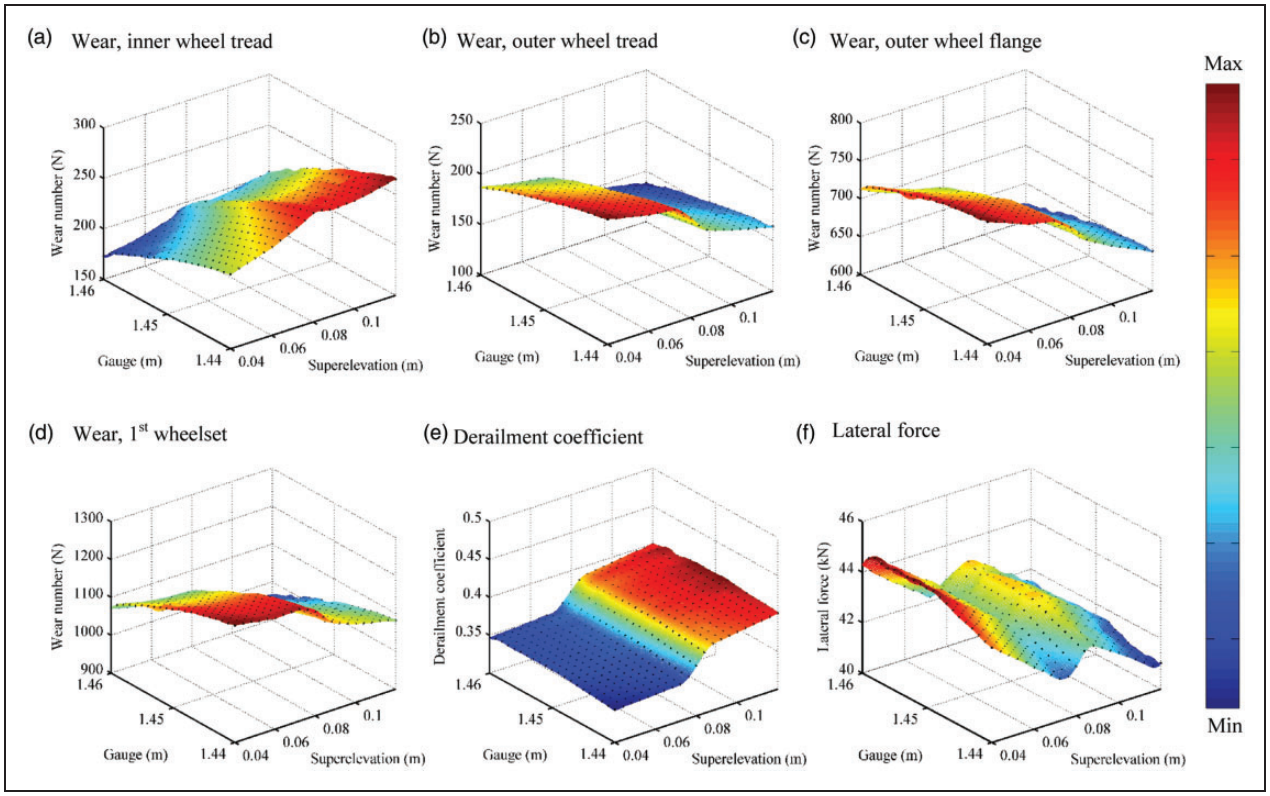

Figure 11. Calculation results when the vehicle negotiates a 375-meter-radius curve with a cant of $\alpha = 1:20$.

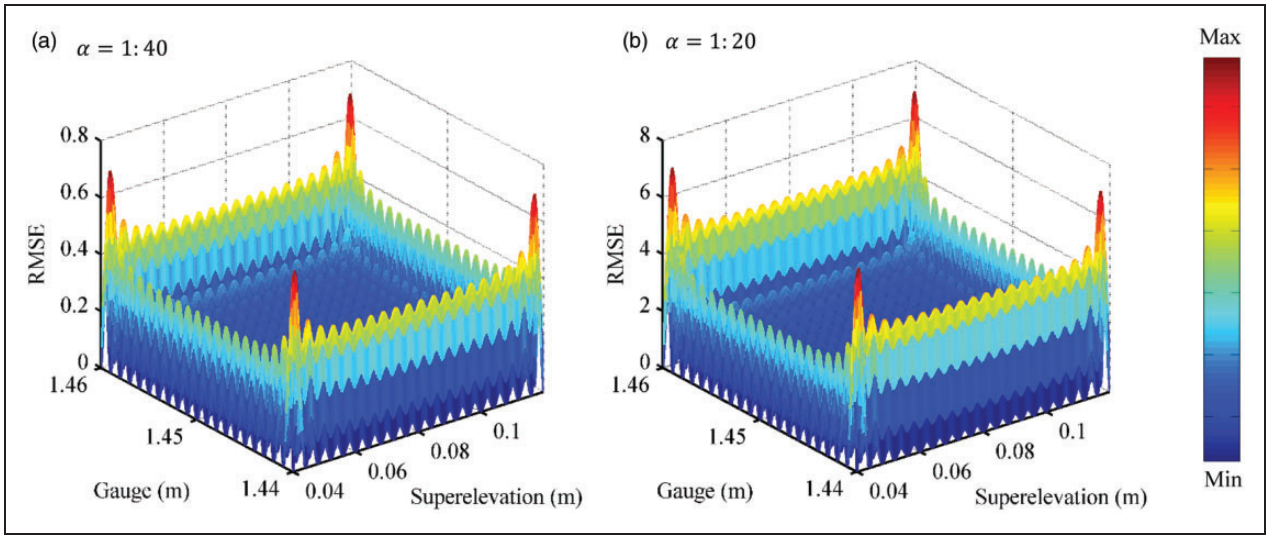

Figure 12. RMSE result over the design space.

guaranteed firstly, where the absolute value of RMSE derived from equation (8) is introduced here. Since our optimization objective is the total wear number of the 1st wheelset, the RSME values of the 1st wheelset under the cant of $\alpha = 1:40$ and $\alpha = 1:20$ are calculated and shown in Figure 12(a) and (b), respectively. These two figures reveal that the error on the edges and corners of the design space is larger than that in the central part. However, these errors can be negligible relative to the results shown in Figures 10(d) and 11(d), which means that the sampling strategy in our work satisfies the designing requirements described in 'Making a sampling plan' section and this KSM model is accurate enough.

To further validate the accuracy of the established KSM, eight different combinations of track layout parameters (4 for $\alpha = 1{:}40$ and 4 for $\alpha = 1{:}20$), which are not involved in the sampling plan, are selected to run dynamics simulations. The total wear numbers of 1st wheelset are generated. Table 2 compares the results calculated by the KSM method and the ones obtained from the dynamics simulations. All the

Table 2. Comparison of the calculated results by KSM and the simulated results through SIMPACK.

Cant	Superelevation (m)	Gauge (m)	Wear number calculated by KSM (N)	Wear number calculated by SIMPACK (N)	Error (%)
1:40	0.054	1.458	109.6	110.2	0.54
	0.083	1.451	117.0	115.8	−1.04
	0.095	1.450	133.8	131.5	−1.95
	0.103	1.444	148.1	149.6	1.00
1:20	0.050	1.457	1095	1098	0.27
	0.063	1.455	1104	1122	1.60
	0.098	1.449	1072	1075	0.28
	0.073	1.444	1178	1175	−0.26

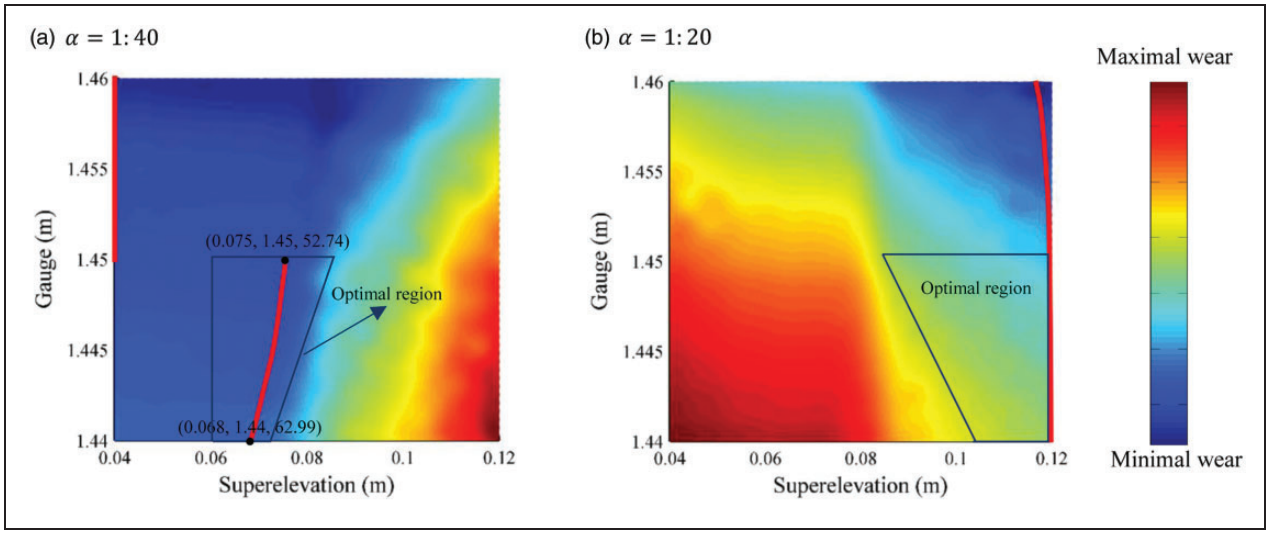

Figure 13. Optimal combination of track layout parameters for reducing W-wear.

errors are lower than 2%. The results thus prove the correctness of the KSM in estimating the wear number.

Track layout optimization based on PSO. In this subsection, according to 'Optimization problem statement' section, PSO is introduced to find the optimal combination of track layout parameters for reducing W-wear. In the automatic optimization, the value of the gauge is first selected, and the superelevation corresponding to the lowest wear, then, is sought by the PSO. Finally, the optimal combination of track layout parameters for reducing W-wear is shown in Figure 13, where the red line represents the optimal combination calculated by PSO.

Figure 13(a) clearly shows that in the case of where the cant is $\alpha = 1:40$, when the gauge is set to $G = 1.440$ m the most suitable superelevation for reducing W-wear is $S = 0.068$ m, and when the gauge is $S = 1.450$ m the most suitable superelevation is $S = 0.075$ m, both values are slightly lower than the equilibrium value ($S = 0.080$ m). If the gauge continues to increase, the optimum superelevation for reducing wear is $S = 0.040$ m, which is much lower than the equilibrium value. Figure 13(b) clearly shows that in the case of where the cant is $\alpha = 1:20$, the optimum superelevation for reducing wear is about $S = 0.120$ m, no matter which range the gauge is in. Both of these two rail cant values show that the W-wear gradually decreases as the gauge widens, which also shows that a proper widening of the gauge can reduce wear (Figures 10(d) and 11(d) show more clearly).

The above results are based on the Sgnss wagon at a speed of 51 km/h. However, in practice, when setting the track layout parameters, the following two issues should be considered.

- When running on the same curve, the speed of different trains may vary. For these trains of different speeds, it is difficult to find a versatile track layout combination that at the same time minimizes the wear of all passing trains.
- To provide a sufficient safety margin, the track layout parameters cannot be changed too large.

Based on the above considerations, and through the simulation results and engineering experience, two suggestion regions concerning track layout for reducing W-wear is given to guide the selection of

Table 3. Calculation results of the wear number and derailment safety indicators for the normal track and the optimized track.

Parameters	Normal track ($S = 0.080$ m, $G = 1.440$, $\alpha = 1{:}40$)	Optimized track ($S = 0.075$ m, $G = 1.450$, $\alpha = 1{:}40$)
Inner WT wear (N)	29.60	28.95
Outer WT wear (N)	70.27	71.22
Outer WF wear (N)	28.13	11.56
Total wear number (N)	128.00	110.29
Derailment coefficient	0.065	0.055
Maximal lateral force (kN)	7.43	7.58

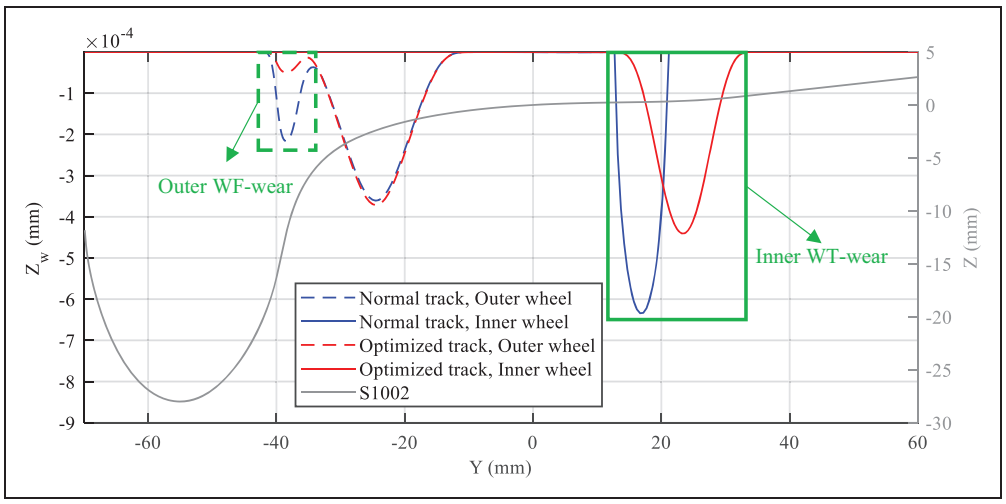

Figure 14. Wear distribution of the 1st wheelset for the normal track and the optimized track.

the track layout parameters, which is called as the optimal region in our work, as shown in Figure 13. Based on these two optimal regions plotted in Figure 13, and the results presented in 'Result analysis' section, the following three suggestions concerning track layout setting are given:

1. For a 350-m-radius curve with a cant of 1:40, it is suggested to select the gauge value from 1.440~1.450 m, and the train is kept in the cant-deficiency running state, and the cant-deficiency amount does not exceed 0.020 m.
2. For a 350-m-radius curve with a cant of 1:20, it is suggested to select the gauge value from 1.440~1.450 m, and the train is kept in the cant-excess running state, and the cant-excess amount does not exceed 0.040 m.
3. It is suggested to use a cant value of 1:40 on the curve as it can greatly reduce the W-wear.

A case study of an optimized track layout

Based on the simulation results from 'KSM-PSO based track layout optimization' section, in this section, two combinations of track layout parameters are introduced for comparison, i.e., an optimized track layout and a normal track layout. Among them, we select the superelevation $S = 0.075$ m, the gauge $G = 1.450$ m, the cant $\alpha = 1{:}40$ as the optimized track, and $S = 0.080$ m, $G = 1.440$ and $\alpha = 1{:}40$ for the normal track. The calculation results, including the wear number and derailment safety indicators, are listed in Table 3. The results show that the W-wear is significantly reduced, with the largest change being the outer WF wear and the reduction in wear number by 58.9%. Besides, the derailment safety is also slightly improved.

To visualize the wear distribution, a wear distribution calculation method that integrates the Hertzian normal contact model,[60] FaStrip tangential contact model[61] and USFD wear model[62] (i.e., Hertzian-FaStrip-USFD[53]) is applied here. The wear distribution after a 1-km journey is shown in Figure 14. When the optimized track is used, two advantages are produced:

1. The outer WF-wear is greatly reduced;
2. The inner WT-wear tends to move outward, and the wear is more uniform.

Base on the comparison results, we can know that the KSM-PSO based track layout parameter optimization method is promising for parameter settings of small-radius curves to reduce W-wear, and of course, can also be used to select the other track geometrical parameters.

Conclusion and discussion

Reducing W-wear has been a topic of great concern since the dawn of railway vehicles. At present, most of the research on W-wear behavior and W-wear reduction is mainly from four aspects: WR tribology, WR profile, vehicle design, and active control of vehicle suspensions. Little attention has been paid to the effects of track layout parameters on W-wear, such as superelevation, gauge, and cant. To supplement the existing research, in our work the effects of track layout parameters (including superelevation, gauge, and cant) on W-wear and derailment safety are analyzed when an Sgnss wagon with a speed of 51 km/h negotiates a 375-m-radius curve of the German Blankenburg-Rübeland railway line, and the following conclusions are obtained.

1. Taking a 375-m-radius curve as a case, the influence of track layout parameters (superelevation, gauge, and cant) on W-wear and vehicle derailment safety is investigated based on the KSM technique. The results show that the track layout parameters have a great influence on W-wear and derailment safety.
2. A KSM-PSO based track layout parameter optimization is proposed, and an optimal combination line is presented. However, when running on the same curve, the speed of different trains may vary. For these trains of different speeds, it is difficult to find a versatile track layout combination that at the same time minimizes the wear of all passing trains. Besides, to provide a sufficient safety margin, the track layout parameters cannot be changed too large. Considering these two aspects and based on practical experience, an optimal region concerning track layout setting for reducing W-wear is presented. This area can provide a reference for the reasonable setting of the track layout parameters.
3. An optimized track is introduced for comparison. The results show that when using the optimized track, the W-wear performance is greatly improved. Specifically, the outer WF-wear is greatly reduced and the inner WT-wear becomes more uniform.

Based on the above results, from the perspective of reducing W-wear, the following measures may be feasible for small-radius curves of rail track.

1. For a 350-m-radius curve with a cant of 1:40, it is suggested to select the gauge value from 1.440~1.450 m, and the train is kept in the cant-deficiency running state, and the cant-deficiency amount does not exceed 0.020 m. This suggestion is also consistent with the modification suggestion proposed in Gao et al.[34]
2. For a 350-m-radius curve with a cant of 1:20, it is suggested to select the gauge value from 1.440~1.450 m, and the train is kept in the cant-excess running state, and the cant-excess amount does not exceed 0.040 m.
3. It is suggested to use a cant value of 1:40 on the curve as it can greatly reduce W-wear.

This study is promising for the parameter setting of those dedicated lines, on which the train speed is usually fixed, such as metro, light rail, and tram. There are two points worth mentioning here.

1. In this paper, the author only analyzes the rail track of a radius of 375 m. For the selection of the track layout parameters of curves with different radii, further study is needed.
2. Changing the track layout parameters will affect W-wear. An in-depth analysis of the mechanism of this phenomenon will be completed in our future work.

Acknowledgements

All resources supporting this work are provided by Fachgebiet Schienenfahrzeuge, TU Berlin.

Declaration of Conflicting Interests

The author(s) declared no potential conflicts of interest with respect to the research, authorship, and/or publication of this article.

Funding

The author(s) disclosed receipt of the following financial support for the research, authorship, and/or publication of this article: The experiment data concerning the railway line and the Sgnss wagon used in this paper are partly supported by the DynoTRAIN project, funded by European Commission (Grant No.: 234079). The first author is also supported by the China Scholarship Council (Grant No.: 201707000113).

ORCID iD

Yunguang Ye https://orcid.org/0000-0002-2921-8420

References

1. Iwnicki S. *Handbook of railway vehicle dynamics*. London: Taylor & Francis, 2006.
2. Lewis R. *Wheel-rail interface handbook*. Boca Raton: CRC Press, 2009.
3. Wang W, Lewis R, Yang B, et al. Wear and damage transitions of wheel and rail materials under various contact conditions. *Wear* 2016; 362-363: 146–152.
4. Li Z, Xing X, Yang M, et al. Investigation on rolling sliding wear behavior of wheel steel by laser dispersed treatment. *Wear* 2014; 314: 236–240.
5. Wang W, Hu J, Guo J, et al. Effect of laser cladding on wear and damage behaviors of heavy-haul wheel/rail materials. *Wear* 2014; 311: 130–136.

6. Lewis S, Lewis R, Evans G, et al. Assessment of railway curve lubricant performance using a twin-disc tester. *Wear* 2014; 314: 205–212.
7. Lu X, Cotter J and Eadie D. Laboratory study of the tribological properties of friction modifier thin films for friction control at the wheel/rail interface. *Wear* 2005; 259: 1262–1269.
8. Santamaria J, Herreros J, Vadillo EG, et al. Design of an optimised wheel profile for rail vehicles operating on two-track gauges. *Vehicle Syst Dyn* 2013; 51: 54–73.
9. Persson I and Iwnicki SD. Optimisation of railway profiles using a genetic algorithm. *Vehicle Syst Dyn* 2004; 41: 517–527.
10. Choi H-Y, Lee D-H and Lee J. Optimization of a railway wheel profile to minimize flange wear and surface fatigue. *Wear* 2013; 300: 225–233.
11. Novales M, Orro A and Bugarín MR. Use of a genetic algorithm to optimize wheel profile geometry. *Proc IMechE, Part F: J Rail and Rapid Transit* 2007; 221: 467–476.
12. Lin F, Zhou S, Dong X, et al. Design method of LM thin flange wheel profile based on NURBS. *Vehicle Syst Dyn* 2019; 1–16.
13. Cui D, Wang R, Allen P, et al. Multi-objective optimization of electric multiple unit wheel profile from wheel flange wear viewpoint. *Struct Multidisc Optim* 2019; 59: 279–289.
14. Firlik B, Staśkiewicz T, Jaśkowski W, et al. Optimisation of a tram wheel profile using a biologically inspired algorithm. *Wear* 2019; 430-431: 12–24.
15. Markine VL, Shevtsov IY and Esveld C. An inverse shape design method for railway wheel profiles. *Struct Multidisc Optim* 2007; 33: 243–253.
16. Shevtsov IY, Markine VL and Esveld C. Optimal design of wheel profile for railway vehicles. *Wear* 2005; 258: 1022–1030.
17. Polach O. Wheel profile design for target conicity and wide tread wear spreading. *Wear* 2011; 271: 195–202.
18. Cui D, Li L, Jin X, et al. Optimal design of wheel profiles based on weighed wheel/rail gap. *Wear* 2011; 271: 218–226.
19. Shen G, Ayasse JB, Chollet H, et al. A unique design method for wheel profiles by considering the contact angle function. *Proc IMechE, Part F: J Rail and Rapid Transit* 2003; 217: 25–30.
20. Ye Y, Sun Y, Dongfang S, et al. Optimizing wheel profiles and suspensions for railway vehicles operating on specific lines to reduce wheel wear: a case study. *Multibody System Dyn* 2020; 1–32.
21. Ignesti M, Innocenti A, Marini L, et al. Development of a wear model for the wheel profile optimisation on railway vehicles. *Vehicle Syst Dyn* 2013; 51: 1363–1402.
22. Zakharov S, Goryacheva I, Bogdanov V, et al. Problems with wheel and rail profiles selection and optimization. *Wear* 2008; 265: 1266–1272.
23. Molatefi H, Mazraeh A, Shadfar M, et al. Advances in Iran railway wheel wear management: a practical approach for selection of wheel profile using numerical methods and comprehensive field tests. *Wear* 2019; 424-425: 97–110.
24. Ye Y, Qi Y, Shi D, et al. Rotary-scaling fine-tuning (RSFT) method for optimizing railway wheel profiles and its application to a locomotive. *Rail Eng Science* 2020; 28: 160–183.
25. Fergusson SN, Fröhling RD and Klopper H. Minimising wheel wear by optimising the primary suspension stiffness and centre plate friction of self-steering bogies. *Vehicle Syst Dyn* 2008; 46: 457–468.
26. Mazzola L, Alfi S and Bruni S. A method to optimise stability and wheel wear in railway bogies. *Int J Railw* 2010; 3: 95–105.
27. Bideleh SMM, Berbyuk V and Persson R. Wear/comfort Pareto optimisation of bogie suspension. *Vehicle Syst Dyn* 2016; 54: 1053–1076.
28. Pérez J, Busturia J and Goodall R. Control strategies for active steering of bogie-based railway vehicles. *Control Eng Pract* 2002; 10: 1005–1012.
29. Matsumoto A, Sato Y, Ohno H, et al. Study on curving performance of railway bogies by using full-scale stand test. *Vehicle Syst Dyn* 2006; 44: 862–873.
30. Markine VL and Shevtsov IY. Optimization of a wheel profile accounting for design robustness. *Proc IMechE, Part F: J Rail and Rapid Transit* 2011; 225: 433–442.
31. Jahed H, Farshi B, Eshraghi MA, et al. A numerical optimization technique for design of wheel profiles. *Wear* 2008; 264: 1–10.
32. Spangenberg U, Fröhling RD and Els PS. Long-term wear and rolling contact fatigue behaviour of a conformal wheel profile designed for large radius curves. *Vehicle Syst Dyn* 2019; 57: 44–63.
33. Liu B, Mei T and Bruni S. Design and optimisation of wheel–rail profiles for adhesion improvement. *Vehicle Syst Dyn* 2016; 54: 429–444.
34. Gao L, Wang P, Cai X, et al. Superelevation modification for the small-radius curve of Shen-Shuo railway under mixed traffic of passenger and freight trains. *Journal of Vibration and Schock* 2018; 35: 222–228.
35. Pombo J, Ambrósio J, Pereira M, et al. A study on wear evaluation of railway wheels based on multibody dynamics and wear computation. *Multibody Syst Dyn* 2010; 24: 347–366.
36. Li Y, Ren Z, Enblom R, et al. Wheel wear prediction on a high-speed train in China. *Vehicle Syst Dyn* 2019; 1–20.
37. Nobari A, Ouyang H and Bannister P. Uncertainty quantification of squeal instability via surrogate modelling. *Mech Syst Signal Process* 2015; 60-61: 887–908.
38. Ye Y, Shi D, Krause P, et al. A data-driven method for estimating wheel flat length. *Vehicle Syst Dyn* 2020; 58: 1329–1347.
39. Chowdhury R and Adhikari S. Fuzzy parametric uncertainty analysis of linear dynamical systems: a surrogate modeling approach. *Mech Syst Signal Process* 2012; 32: 5–17.
40. Simpson TW, Mauery TM, Korte J, et al. Kriging models for global approximation in simulation-based multidisciplinary design optimization. *AIAA J* 2001; 39: 2233–2241.
41. Fateh MM and Zirkohi MM. Adaptive impedance control of a hydraulic suspension system using particle swarm optimisation. *Vehicle Syst Dyn* 2011; 49: 1951–1965.
42. Baeza L, Fayos J, Roda A, et al. High frequency railway vehicle-track dynamics through flexible rotating wheelsets. *Vehicle Syst Dyn* 2008; 46: 647–659.
43. Han J, Zhong S, Xiao X, et al. High-speed wheel/rail contact determining method with rotating flexible

wheelset and validation under wheel polygon excitation. *Vehicle Syst Dyn* 2018; 56: 1233–1249.
44. Hecht M, Keudel J and Friedrich D. Dokumentation der Messfahrten aus Juni 2006. Technische Universität Berlin, 2006. Report No. 12/2006.
45. Ye Y, Shi D, Krause P, et al. Wheel flat can cause or exacerbate wheel polygonization. *Vehicle Syst Dyn* 2019; 1–32.
46. Hecht M and Keudel J. Numerische simulation eines Selbstentladewagens mit Y25-Drehgestellen. Technische Universität Berlin, 2005. Report No. 31/2005.
47. Schelle H and Hecht M. Fahrtechnische zulassung: Einfluss von randbedingungen in der simulation. *ZEVrail* 2018; 137: 307–313.
48. Schelle H. *Radverschleißreduzierung für eine Güterzuglokomotive durch optimierte Spurführung*. Doctoral dissertation, Technische Universität Berlin, 2014.
49. Profillidis VA. *Railway engineering*. Aldershot: Avebury Technical, 2000.
50. Pearce T and Sherratt N. Prediction of wheel profile wear. *Wear* 1991; 144: 343–351.
51. Zobory I. Prediction of wheel/rail profile wear. *Vehicle Syst Dyn* 1997; 28: 221–259.
52. Braghin F, Lewis R, Dwyer-Joyce R, et al. A mathematical model to predict railway wheel profile evolution due to wear. *Wear* 2006; 261: 1253–1264.
53. Tao G-q, Du X, Zhang H-j, et al. Development and validation of a model for predicting wheel wear in high-speed trains. *J Zhejiang Univ Sci A* 2017; 18: 603–616.
54. Enblom R. Deterioration mechanisms in the wheel–rail interface with focus on wear prediction: a literature review. *Vehicle Syst Dyn* 2009; 47: 661–700.
55. Peng B, Iwnicki S, Shackleton P, et al. Comparison of wear models for simulation of railway wheel polygonization. *Wear* 2019; 436–437: 203010.
56. UIC Code 518 OR 2009. *Testing and approval of railway vehicle from the point of view of their dynamic behavior – safety – track fatigue – running behavior*. Paris: International Union of Railway, 2009.
57. Jiaqiang E, Han D, Qiu A, et al. Orthogonal experimental design of liquid-cooling structure on the cooling effect of a liquid-cooled battery thermal management system. *Appl Therm Eng* 2018; 132: 508–520.
58. Roshanian J and Ebrahimi M. Latin hypercube sampling applied to reliability-based multidisciplinary design optimization of a launch vehicle. *Aerosp Sci Technol* 2013; 28: 297–304.
59. Xin C, Lu Q, Ai C, et al. Optimization of hard modified asphalt formula for gussasphalt based on uniform experimental design. *Constr Build Mater* 2017; 136: 556–564.
60. Hertz H. Über die berührung fester elastische körper. *J Die Reine Angewandte Math* 1982; 92: 156–171.
61. Sichani MS, Enblom R and Berg M. An alternative to FASTSIM for tangential solution of the wheel–rail contact. *Vehicle Syst Dyn* 2016; 54: 748–764.
62. Lewisa R and Dwyer-Joyce RS. Wear mechanisms and transitions in railway wheel steels. *Proc IMechE, Part J: J Engineering Tribology* 2004; 218: 467–478.

Appendix

Notation

a^+	half wheelset base
a^*	half pivot distance
c_{by}, c_{bz}	ballast damping
c_c	contact damping
c_{fy}, c_{fz}	fastener damping
c_{sx}, c_{sy}, c_{sz}	secondary suspension damping
CMA-ES	covariance matrix adaptation evolution strategy
D	wheel rolling circle diameter
DOFs	degrees of freedom
f_{wear}	wear number
$f^T(\mathbf{x})$	regression model
F_x, F_y	creep force
G	track gauge
GC	gauge corner
GA	genetic algorithm
I_{axx}	axlebox roll moment of inertia
I_{ayy}	axlebox pitch moment of inertia
I_{azz}	axlebox yaw moment of inertia
I_{bxx}	bogie frame roll moment of inertia
I_{byy}	bogie frame pitch moment of inertia
I_{bzz}	bogie frame yaw moment of inertia
I_{cxx}	carbody roll moment of inertia
I_{cyy}	carbody pitch moment of inertia
I_{czz}	carbody yaw moment of inertia
I_{wxx}	wheelset roll moment of inertia
I_{wyy}	wheelset pitch moment of inertia
I_{wzz}	wheelset yaw moment of inertia
k_{by}, k_{bz}	ballast stiffness
k_c	contact stiffness
k_{fy}, k_{fz}	fastener stiffness
KSM	Kriging surrogate model
LHS	Latin hypercube sampling
m_a	axlebox mass
m_b	bogie frame mass
m_v	vehicle frame mass
m_w	wheelset mass
m_s	sleeper mass
MBS	multibody dynamics simulation
MSE	mean squared error
P_0	static axle load
PSO	particle swarm optimization
Q	wheel-rail lateral force
r	track radius
$r(x)$	correlation function vector of the sample point
$\mathbf{r}$	correlation matrix
R	spatial correlation between the sample points
$\mathbf{R}$	spatial correlation matrix
RCF	rolling contact fatigue
RH	rail head
RRD	rolling radius difference
RMSE	root mean square error

S_e	equilibrium superelevation
SM	surrogate model
t	time
T	tangential force
USFD	University of Sheffield
v	vehicle speed
v_x, v_y	creepage
WF	wheel flange
WR	wheel-rail
WT	wheel tread
W-profile	wheel profile
W-wear	wheel wear
x_i	a point of a sample
$\mathbf{x}$	an input sample
$\mathbf{X}$	input sample point group
$y(\mathrm{x})$, $\hat{\mathrm{y}}(\mathrm{x})$	predicted response
Y	wheel-rail vertical force
$Y_{2\mathrm{m}}$	lateral force-sliding mean over 2 m of the track
$\mathbf{Y}$	output sample point group
$Z(\mathbf{x})$	random Gaussian distribution
α	rail cant, or wheel flange angle
$\boldsymbol{\beta}$, $\hat{\boldsymbol{\beta}}$	undetermined coefficient
γ	creepage
θ	active vector
θ_l	the lth component of θ
μ	friction coefficient
υ	Poisson ratio
σ^2, $\hat{\sigma}^2$	variance